Estimating the Evaporative Cooling Bias of an Airborne Reverse Flow Thermometer

YONGGANG WANG AND BART GEERTS

University of Wyoming, Laramie, Wyoming

(Manuscript received 25 February 2008, in final form 24 June 2008)

ABSTRACT

Airborne reverse flow immersion thermometers were designed to prevent sensor wetting in cloud. Yet there is strong evidence that some wetting does occur and therefore also sensor evaporative cooling as the aircraft exits a cloud. Numerous penetrations of cumulus clouds in a broad range of environmental and cloud conditions are used to estimate the resulting negative temperature bias. This cloud exit ''cold spike'' can be found in all cumulus clouds, even at subfreezing temperatures, both in continental and maritime cumuli. The magnitude of the spike correlates most strongly with the dryness of the ambient air. A temperature correction based on this relationship is proposed. More important than the cloud exit cold spike, from a cumulus dynamics perspective, is the negative bias *within* cloud. Such bias is expected, due to evaporative cooling as well. Evaporation from the wetted sensor in cloud is surmised because air decelerates into the thermometer housing, and thus is heated and becomes subsaturated. Thus an in-cloud temperature correction is proposed, based on the composite cloud exit evaporative cooling behavior. This correction leads to higher and more realistic estimates of cumulus buoyancy and lower estimates of entrainment.

1. Introduction

Cumulus clouds are driven by buoyancy. Buoyancy is notoriously difficult to measure (e.g., LeMone 1980), and this hampers our understanding of cumulus dynamics. Cloud buoyancy is affected by water loading, pressure, and water vapor perturbations, but it is usually dominated by temperature perturbations. Also, the accurate measurement of temperature variations in cumuli is essential to understand entrainment (Paluch 1979; Jonas 1990; Blyth 1993).

Two types of temperature probes are used on aircraft, radiometric, and immersion thermometers. The latter type uses a sensor immersed in the airstream, for instance the commonly used Rosemount thermometer. The exposure of the sensing element, usually a platinum wire, to a stream of water droplets yields an anomalously low temperature in cloud and mainly as the aircraft exits the cloud (Heymsfield et al. 1979; LeMone 1980). Rain below cloud base may also cause instrument wetting and thus evaporative cooling below the air temperature (Eastin et al. 2002). At subfreezing temperatures, ice may accrete on the sensor, thus temperature underestimation may occur long after exiting the cloud, and in fact some immersion thermometer sensors are intermittently heated to prevent ice accumulation. The Rosemount probe has been used in several cumulus dynamics studies, including McCarthy (1974), LaMontagne and Telford (1983), and Jonas (1990). Estimated typical magnitudes of the Rosemount temperature underestimate in cloud range from 0.5 (Nicholls et al. 1988) to 1.5 K (Eastin et al. 2002).

These errors led to the design of a reverse flow thermometer (RFT), in which the sensor is shielded in a housing through which the air flows in the direction opposite to the airstream (Rodi and Spyers-Duran 1972). This reduces wetting or icing of the sensor (Heymsfield et al. 1978). Yet there is evidence that reverse-flow immersion thermometers still become wet in cumulus clouds (Lawson and Rodi 1987). This leads to erroneously low temperatures upon exiting a cloud because of evaporative cooling (Lawson and Cooper 1990, hereafter referred to as LC90). This error does not exclusively occur just outside cloud, where it is most obvious, but also in cloud, because the airstream adjacent to the sensor has been dynamically heated during its deceleration in the RFT housing (Lenschow and Pennell 1974). The dynamic heating is a function of the ratio of the decelerated flow speed to the true airspeed (known as the ''recovery factor'') and can be accurately

Corresponding author address: Bart Geerts, Department of Atmospheric Sciences, University of Wyoming, Laramie, WY 82071. E-mail: geerts@uwyo.edu

DOI: 10.1175/2008JTECHA1127.1

© 2009 American Meteorological Society

corrected for. Cloudy air that is aerodynamically heated is no longer saturated in the immediate vicinity of the sensor, because the time scale for cloud droplets to respond to changes in ambient humidity is much larger than the travel time through the RFT housing (Politovich and Cooper 1988). Thus if water is present on the sensor, it will evaporate, cooling the sensor toward the wet-bulb temperature of the heated air.

An RFT is currently used on the University of Wyoming King Air (WKA), a National Science Foundation research aircraft. Several other aircraft use or have used an RFT as part of their instrument suite, including the National Center for Atmospheric Research (NCAR) Queen Airs, King Air, and Electra.

The purpose of this study is to quantify the RFT evaporative cooling (EC) bias in cumulus clouds, develop a correction for the EC error both inside and just outside cumulus, and thus to obtain better estimates of cumulus buoyancy and entrainment. The in-cloud correction is based on the much larger EC bias in the exit region of cumulus clouds. We examine how this EC bias is affected by ambient (out of cloud) and microphysical (in cloud) conditions. The correction is empirical and has become possible owing to a large number of cumulus penetrations flown in recent years in a broad range of ambient conditions.

An example of a cloud exit EC error is shown in Fig. 1. The WKA penetrated a visibly growing tower with sharp edges and with a 5 m s^{-1} peak updraft (Fig. 1b). The extent of the cumulus cloud can be inferred from the cloud droplet number concentration N_o and the liquid water content (LWC). The reverse flow temperature (TRF) trace shows a downward spike at the cloud exit point, and a gradual recovery afterward. This evolution is not related to changes in aircraft altitude (not shown). The recovery appears to be exponential, suggesting that most droplets on the temperature sensor evaporate quickly in the dry airstream, while the larger ones need more time. The negative TRF spike and exponential recovery are common features of cumulus exit regions. We are aware that a real negative temperature anomaly may occur along the cloud edges, for example, due to the evaporation of cloud droplets in detrained air (e.g., Jonas 1990). For instance, the cold anomaly seen near the entrance of the cumulus in Fig. 1 (at $x = 0.78$ km) may be real.

The analysis method and data sources are introduced in section 2. The cloud exit EC bias is quantified and related to cloud and ambient conditions in section 3. The adaptation of the proposed cloud exit EC correction for use within clouds is presented in section 4, and the impact of this correction on cumulus buoyancy and entrainment is discussed in section 5.

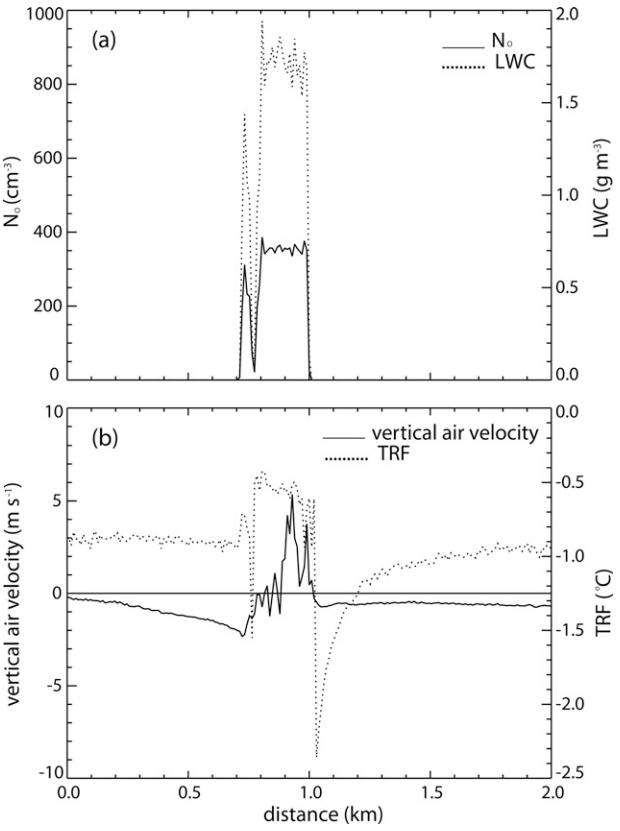

FIG. 1. WKA measurements of a cumulus penetrated during CuPIDO-06 at 1707 UTC 24 Jul 2006. (a) FSSP cloud droplet number concentration (N_o) and LWC; (b) vertical air velocity and TRF. The flight direction in this figure and all other transects shown in this paper is from left to right.

2. Method and data sources

A large number of cumulus clouds were penetrated by the WKA in three recent campaigns: 72 h were flown in the High-Plains Cumulus (HiCu-03) campaign in Wyoming in the summer of 2003, mostly in cumulus congestus with a cloud base near the freezing level (Damiani et al. 2006). A further 89 h were flown in the Rain in Cumulus over the Ocean (RICO-04) campaign (Rauber et al. 2007), conducted in shallow precipitating trade wind cumuli over the tropical North Atlantic Ocean in winter. And 60 h were flown in shallow–deep orographic convection in Arizona in summer as part of the Cumulus Photogrammetric, In-Situ and Doppler Observations (CuPIDO-06) campaign (Damiani et al. 2008; Geerts et al. 2008). Typical conditions of the sampled cumulus clouds in these three campaigns are listed in Table 1. The cloud droplet number concentration N_o is obtained from the Forward Scattering Spectrometer Probe (FSSP). This count can, in theory, include ice crystals, but the ice crystal concentration is

TABLE 1. Basic cloud properties and cloud exit EC parameters for all cumuli used in this study, in three campaigns. Cumulus depths were estimated from the zenith antenna of the WCR and the lifting condensation level. The quality of fit is discussed in the text.

	HiCu-03	RICO-04	CuPIDO-06
Environment	Continental	Maritime	Continental
Number of clean cloud exit samples ($T > -12.3$°C)	77	153	76
Number of clean cloud entrance samples ($T > -12.3$°C)	291	188	162
Mean in-cloud temperature before EC correction (°C)	−9.0	+15.5	+0.6
Approx range of cumulus depths (km)	1.0–3.8	0.8–2.7	0.7–10
Mean cloud droplet number concentration (cm^{-3})	446	56	216
Mean droplet diameter (μm)	8.6	19.2	16.3
Mean cloud liquid water content ($g\ m^{-3}$)	0.35	0.43	0.83
Quality of cloud exit EC bias fit (K)	0.088	0.094	0.101
Mean cloud exit EC amplitude ΔT_o (K)	−0.77	−1.07	−1.75
Mean cloud exit EC time constant τ_d (s)	2.20	2.33	1.88
Standard error of the regression estimate of ΔT_o (K)	0.70	0.76	0.80

orders of magnitude smaller than the typical droplet concentration. The cloud liquid water content is inferred from the same probe, by integrating over all droplet size bins (Brenguier et al. 1994). It does not include drizzle or raindrops, but the FSSP LWC generally compared well (within 10%) with that from the Gerber particle volume monitor (PVM-100) (Gerber et al. 1994) and the DMT-100 (Droplet Measurement Technologies) hotwire probe (King et al. 1981) for all three field campaigns. Clearly, the HiCu-03 cumuli were the most ''continental,'' with the highest N_o, the lowest LWC, and the smallest mean droplet diameter. CuPIDO-06 took place during the North American monsoon; these cumuli had a remarkably high LWC and, in terms of droplet size distribution and number concentration, they were intermediate between the unpolluted maritime cumuli east of the Lesser Antilles in RICO-04 and the truly continental HiCu-03 cumuli. Most clouds in the three campaigns were cumuli congesti. Most clouds also contained some liquid or frozen precipitation, according to cloud radar data collected on all flights. All RICO-04 target clouds were relatively shallow clouds with tops below the freezing level, while the CuPIDO-06 cumuli ranged in size from cumulus humilis to cumulonimbus. As will be shown later, the combination of the three campaigns covers a broad range of cloud microphysical and ambient temperature and humidity conditions.

The instrument of primary interest in this study is the reverse flow thermometer (Fig. 2). The dynamic heating from the free airstream to the platinum wire sensor amounts to about 2.3 K for the typical WKA true airspeed (~90 $m\ s^{-1}$) and the specific recovery factor of the probe aboard the WKA. It is not clear how the wetting of the sensor occurs. Wind tunnel observations reported by LC90 indicate that drops are collected on

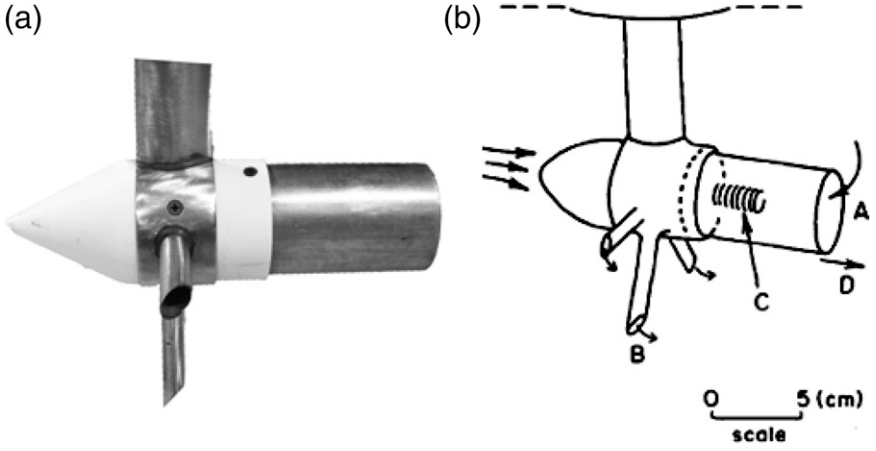

FIG. 2. Photo and schematic of the reverse-flow thermometer. Air enters through port (A) and exits through any of several ports (B). Inside the housing, the air flows past a platinum wire sensor (C) wound in a spiral, 25 μm in diameter. The reverse-flow design is intended to separate hydrometeors (D) from the airstream that enters the probe. The schematic on the right is from LC90.

the outside of the RFT housing. This water then travels rearward until reaching the round opening in the back (''A'' in Fig. 2) and then accumulates just inside the cylinder. The reverse airflow is very turbulent, and some of this accumulated water is caught in the turbulence and sprayed onto the sensor. Our measurements indicate that this wetting happens quickly; even clouds less than 100 m wide can produce a cloud exit EC signature, but stronger EC signatures occur at the exit of clouds at least a few 100 m wide. Wind tunnel observations (LC90) suggest that at temperatures below freezing, supercooled water accretes at the leading edge of the thermometer housing and does not travel to the trailing edge.[1] Based on these observations, LC90 speculated that the cloud exit EC error should vanish at temperatures below freezing. Heymsfield et al. (1978) illustrate rime accumulation on the leading edge of the RFT probe in a wind tunnel, and our own field observations during HiCu-03 and CuPIDO-06 confirm this. But as will be shown later, the EC bias at the cloud exit does occur below freezing, in fact even at air temperatures well below −2.3°C (corresponding with 0°C within the RFT housing). This suggests that at least some sensor wetting results from droplets that never contact the housing but remain embedded in the turbulent reverse flow. Presumably only the smallest droplets are not separated out at the RFT trailing edge.

Cumulus clouds can be quite ragged, and clear definitions of a cloud and a cloud exit are needed. Only (roughly) level aircraft penetrations through cumuli are included. Cloud definitions are based on the FSSP N_o measurements at 10 Hz, corresponding with a spatial resolution of about 9 m. Data from all other probes are measured at a higher frequency and are reduced to a common frequency of 10 Hz. A cloud is defined as a region at least 200 m wide with average N_o values exceeding a critical value $N_{o,c}$. For continental cumuli (HiCu-03 and CuPIDO-06), $N_{o,c} = 100$ cm^{-3}, and for maritime cumuli (RICO-04), $N_{o,c} = 50$ cm^{-3}. Pockets of lower droplet concentrations ($N_o < N_{o,c}$) in cloud are allowed, but their maximum width is 100 m, as is the case for the cumulus in Fig. 1.

The resulting population of clouds then is used to obtain a sample of ''clean'' cloud edges, defined as the first point where $N_o < 1$ cm^{-3} and N_o does not exceed 50 cm^{-3} (20 cm^{-3} for RICO-04) anywhere over a distance of at least 800 m in front of (for entrances) or behind (for exits) the cloud. Only clean entrances and exits are used in this study, because small patches of cloud in the exit region can produce their own cloud exit EC signal or at least contaminate the temperature recovery following cloud exit from the main cloud (Fig. 3). Clearly only a fraction of clouds has clean exits. It is worth noting that the number of clean exits is smaller than the number of clean entrances (Table 1). The reason for this probably is that the pilot tended to penetrate a cumulus at a point where the cloud edge was well defined, near the center of the cloud as judged during the approach. The pilot cannot know what the cloud exit region looks like.

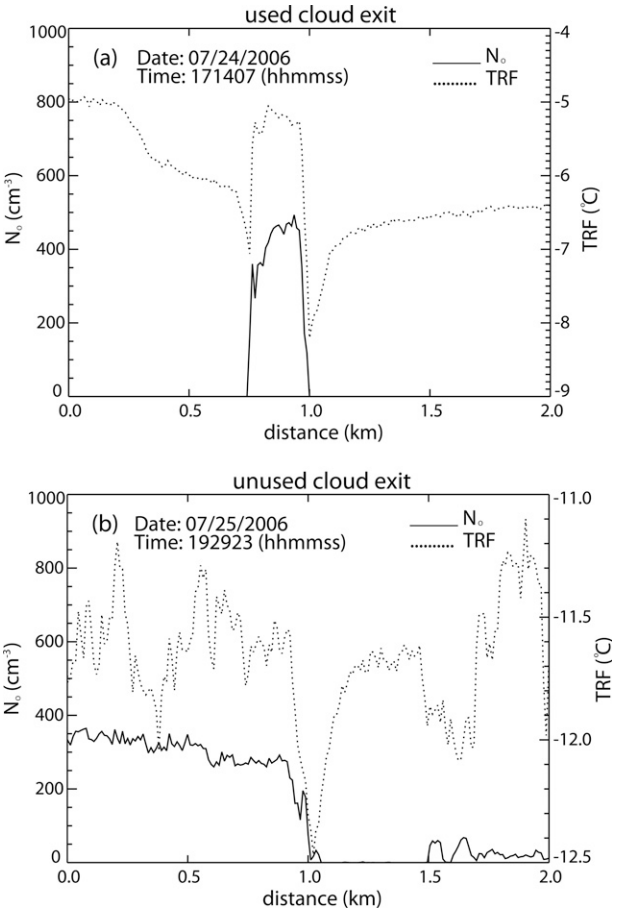

FIG. 3. Sample cloud exits from CuPIDO-06: (a) used and (b) unused. The cloud edge in (b), at a distance of 1.0 km, is followed by a thin cloud within 800 m; therefore, it is rejected. The cloud edge in (a) is considered ''clean'' and is included in the study.

3. Estimating the evaporative cooling bias in the cloud exit region

a. Composite temperature trace

The composite TRF traces for all entrances and all exits for the three experiments are shown in Fig. 4. The

[1] Note that no components of the RFT probe are heated to remove accreted ice.

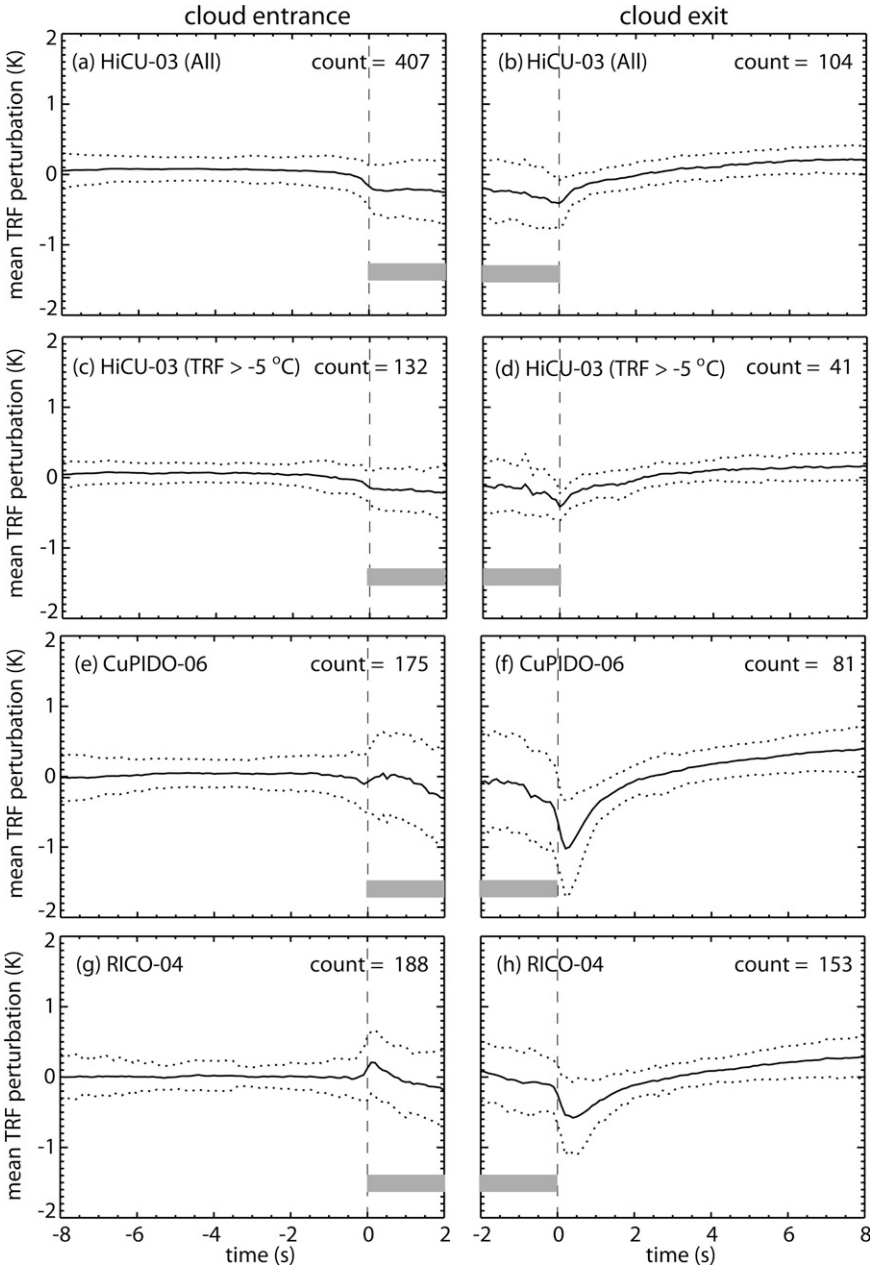

FIG. 4. Composite TRF traces for all clean cloud entrances and exits for (a), (b) HiCu-03; (c), (d) HiCu-03 (only those penetrations with TRF > -5°C); (e), (f) CuPIDO-06; and (g), (h) RICO-04. The number of samples for each composite is shown as ''count.'' The TRF values are perturbations from the 10-s means. Solid lines denote the average, dashed lines the average ± 1 std dev. The flight direction is from left to right. The wide gray bar in this figure, as well as in the following figures, indicates the cloudy region, and the dashed vertical lines are the cloud edges.

composites are obtained by removing the mean temperature for a 10-s section (2 s in cloud, 8 s out of cloud) for each cloud edge region, and by averaging this perturbation temperature over all clean cloud edges, at a given distance (or rather, time) from the cloud edge. The logic for contrasting exit regions with entrance regions is as follows: true cooling at the exit of a cumulus cloud is quite possible, as mentioned before, but that cooling should not depend on the way the aircraft penetrated the cloud: if the sample size is statistically sig-

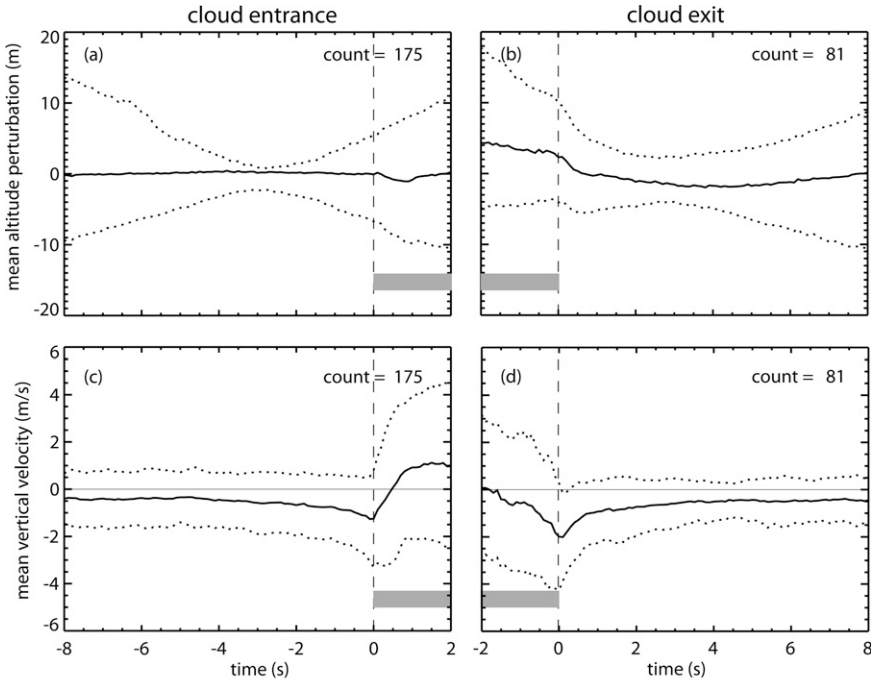

FIG. 5. Composite trace of aircraft (a), (b) perturbation altitude and (c), (d) vertical air velocity for all clean cumulus: (a), (c) entrances and (b), (d) exits in CuPIDO-06. The vertical air velocity is obtained from the gust probe.

nificant, the difference in temperature trend between exit and entrance regions should be entirely instrument related. This is because in all three experiments, cumuli were penetrated from various angles. Usually a penetration was repeated in the opposite direction, or else the cumulus was penetrated more than twice following a rosette flight pattern (Damiani et al. 2008).

The composite TRF trace has a clear negative spike just behind the cloud exit followed by a more gradual recovery, at least for CuPIDO-06 (Fig. 4f) and RICO-04 (Fig. 4h). This signature is not present near entrance regions. Three explanations are offered: there are systematic variations in aircraft altitude associated with cumulus drafts; the aircraft typically penetrated the cumulus in the direction of the wind shear; and the EC of a wetted sensor. The first and third explanation regard the cold spike as an error, related to the instrument or the platform; the second explanation regards the cold spike as physically real.

Regarding the first explanation, if the cloud exit cold spike is due to changes in aircraft altitude, then the aircraft should, on average, quickly climb upon exiting a cumulus and then gradually recover to its assigned altitude. The brief, rapid ascent could be due to persistent downdrafts in the sampled cumuli, forcing the (auto)pilot into climb mode within cumulus. The composite measurements show, first, that updrafts are more common than downdrafts in the sampled Cu, except along the cumulus edges, where downdrafts prevail (Figs. 5c,d); second, the resulting variation in the aircraft altitude is very small, less than 10 m on average (Figs. 5a,b). Instead of climbing, the aircraft typically sank by a few meters upon exiting a cumulus. A 5-m descent of the aircraft results in at most a 0.05-K warming. This is an upper estimate since the lapse rate is typically smaller than dry adiabatic in Cu and in the environment. The observed temperature anomaly in cloud exit regions tends to be much larger (0.5–1 K; Fig. 4), and it is of the opposite sign. This rules out the altitude theory. For completeness, we did correct the TRF values for aircraft altitude variations in both entrance and exit regions by computing departures from the 10-s mean height, and assuming a lapse rate of 6 K km^{-1}. In other words, we brought the TRF data to a common height for each flight segment before further processing.

Second, it can be argued that the tendency for cooler air to occur in exit regions is due to the evaporation of droplets in the detrained air, leading to negative buoyancy and a cloud-edge region of sinking air (Fig. 5d). This would happen in the entrance region as well, but if the aircraft tends to approach cumuli from the upshear side where the cloud edge tends to be better defined, then one expects more cooling and stronger subsidence

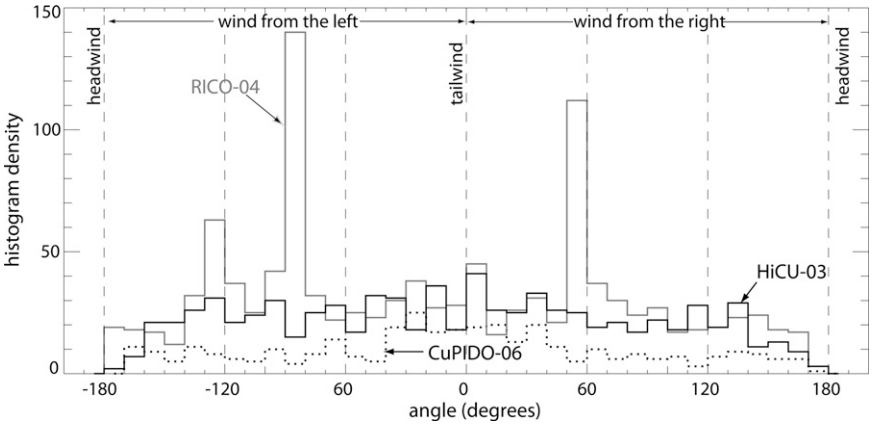

FIG. 6. Histogram of the angle between the flight-level wind direction and the aircraft heading, for all cumulus penetrations in the three campaigns.

on average in the exit region (i.e., usually on the downshear side). Indeed, clean edges are more common on the entrance side than the exit side in all three campaigns (Fig. 4), and the average exit region downdraft (Fig. 5d) peaks at -2 m s^{-1}, which is stronger than the entrance region downdraft (Fig. 5c). Cumuli were penetrated from every angle, however, and the most common direction differed between the three campaigns (Fig. 6). Overall, tailwind approaches (a surrogate for an approach from the upshear side) are not significantly more common than headwind approaches.

That leaves only the third explanation, that is, the cloud exit cold spike is due to EC on the RFT sensor. The composite TRF trace for HiCu-03 shows some cooling at the exit (Fig. 4b), but not the clear spike seen in the two other campaigns. The main reason for this is that many HiCu-03 cumulus penetrations occurred at temperatures below -5°C (Table 1). The composite TRF trace for the warmer HiCu-03 cases (>-5°C) shows a cleaner negative spike and exponential recovery in the exit region (Fig. 4d), although the cold spike amplitude is smaller than for the two other campaigns, and the cold spike location is closer to the cloud edge. Several individual HiCu-03 penetrations do show a clear cooling spike.

Another observation evident in Fig. 4 is that in all three campaigns TRF tends to decrease as the aircraft enters the cloud. This cooling tends to continue across the cloud, not just in the first 2 s of cloud shown in Figs. 4a,c,e,g, but all the way to the exit point (i.e., between -2 and 0 s in Figs. 4b,d,f,h). This apparent cooling can be seen also in the individual (noncomposite) complete-cloud cumulus transects shown in Heymsfield et al. (1979), in LC90, and in many CuPIDO cases (e.g., Fig. 1b). One expects cumulus towers to be warmer than the surroundings, at least between the level of free convection and the level where the entraining clouds become neutrally buoyant. Penetrations were made at all levels of the cumuli, always below anvils, and at all stages of the lifetime of individual towers and of cumulus clusters. In particular for the RICO-04 cumuli, the RFT does register a higher temperature upon entrance (Fig. 4g), but after less than 0.5 s in cloud, a cooling trend sets in.

This cooling trend, or more generally the discordance between the composite TRF trace in the first 200 m in cloud and that in the last 200 m in cloud (Fig. 4), is the strongest argument for the hypothesis that EC occurs at the RFT sensor *within* cloud. The theoretical limit of the TRF cooling due to evaporation is the wet-bulb temperature depression of the dynamically heated air (LC90). At the airspeed of the WKA, this depression within cloud, where the air is assumed to be saturated ($T_r - T_{w,\mathrm{cr}}$ in Fig. 7a), is about 1.4 K at an ambient temperature of 20°C and 0.6 K at -10°C (Fig. 8). The theoretical limit of the cloud exit cold spike (i.e., the wet-bulb depression of the ambient air) is much larger, especially in warm, dry air (Fig. 8). This limit is rarely reached in the exit region, however, because the sensor is no longer actively wetted.

As mentioned in section 2, LC90 speculated that cloud exit EC of the RFT should cease at temperatures below 0°C, because supercooled water freezes upon contact with the RFT housing, building up rime on the leading cone. The variation of the cloud exit cold spike with ambient temperature is examined in Fig. 9. At temperatures below -12.3°C, the cloud exit cold spike is weaker compared to that at higher temperatures, but not absent. It is possible that under the high accretion rate of supercooled water on the RFT housing, the heat exchange is insufficient to freeze all the water, and that some water still travels rearward and is shed from the

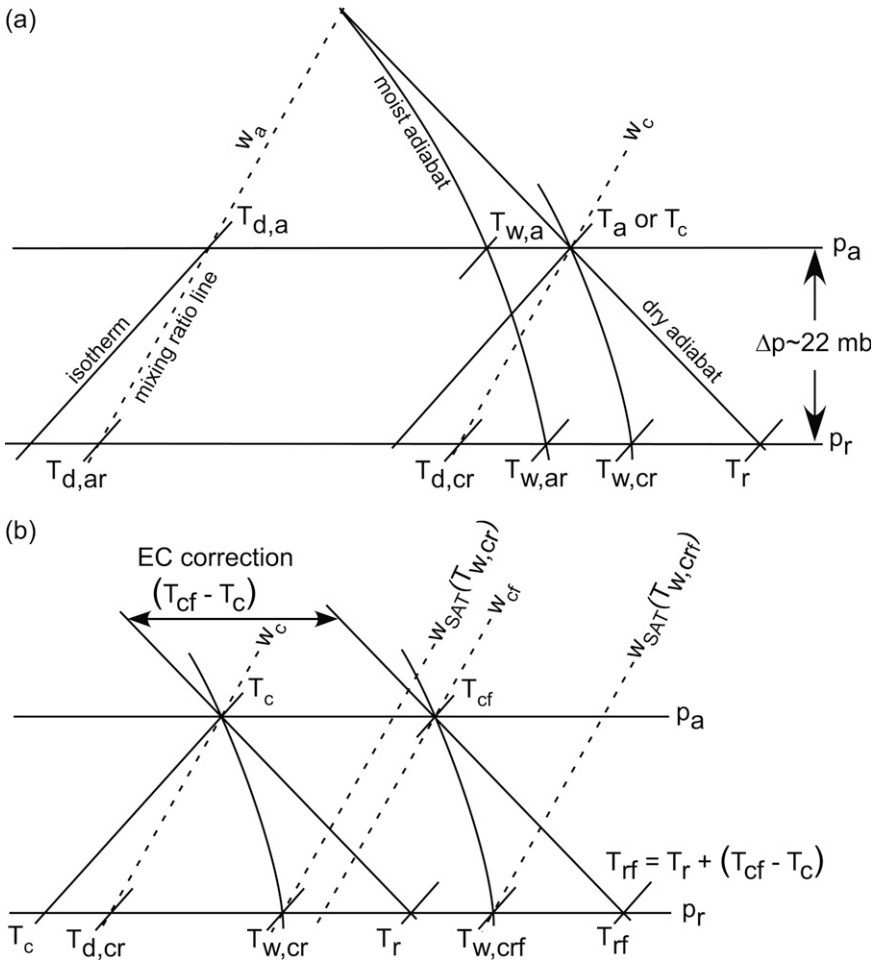

FIG. 7. Temperature relationships sketched on a skew T–log$p$ diagram (a) for both clear air and cloud conditions, and (b) for the in-cloud EC correction method. Subscript a refers to nonsaturated air, subscript c to cloudy air, subscript r to conditions inside the RFT housing, and subscript f to the ''final'' values resulting from the iterative EC correction in cloud. The temperature, dewpoint, and wet-bulb temperature are denoted as T, T_d, and T_w, respectively, w stands for mixing ratio, and p stands for pressure. It is assumed that the compression of air as it enters the RFT housing is dry adiabatic, even if cloud droplets are present.

rear of the RFT cylinder. Many of the cloud exit cases below −7.3°C have a very low mean cloud LWC (0.1–0.2 g m^{-3}), and they still show a minimum near the exit point and a gradual TRF recovery. This suggests that at any temperature at least some of the water reaching the platinum wire is not shed from the RFT housing, but rather remains suspended in the airstream as it travels through the reverse flow tube. The higher latent heat of sublimation (rather than the latent heat of evaporation) and the lower vapor pressure deficit of the ambient air relative to ice (compared to water) may explain the longer recovery time for the two lowest temperature ranges in Fig. 9 and for other cases shown below.

Given the gradual decrease in TRF cloud exit cold spike magnitude with decreasing ambient temperature below −2.3°C (Fig. 9), we will implement the RFT EC correction (discussed below) gradually between −12.3° and −2.3°C.

b. *Quantification of the TRF bias in the cloud exit region*

The TRF *bias* ΔT at cloud exit, due to evaporative cooling at the surface of the wetted sensor, can be approached by an exponential decay curve:

$$\Delta T = \Delta T_o \exp\left(-\frac{t}{\tau_d}\right) \qquad 0.2 < t < 8.0\,\text{s}, \quad (1)$$

where ΔT is the difference between the TRF at a particular time t and the temperature after recovery. The

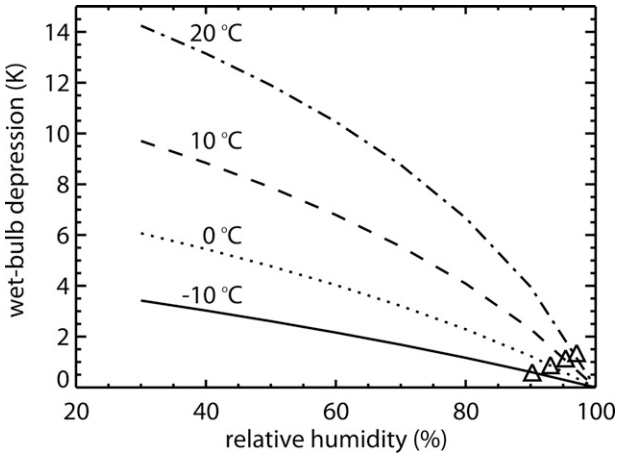

FIG. 8. Variation of the wet-bulb depression with relative humidity and temperature at a pressure of 700 hPa. The triangles represent conditions in the RFT housing, at four different temperatures.

latter is a reference temperature, and is defined as the mean TRF value between 6 and 8 s beyond the cloud exit (Fig. 10). The corresponding distance (approximately 540–720 m from the cloud edge) is chosen as a trade-off between two requirements: (i) all droplets should have evaporated from the RFT sensor, and (ii) this distance should represent conditions just outside the cloud.

The two unknowns in (1), ΔT_o and τ_d, are the amplitude of cloud exit EC bias and the drying time constant, respectively. They are determined by means of a least squares linear fit of the observed against the modeled $\ln(\Delta T)$ in the time domain shown in Eq. (1). Any immersion thermometer has some time delay (or time response) due to the characteristics of the flow and the sensing wire. According to Spyers-Duran and Baumgardner (1983), the RFT attains 90% of the signal at 0.15 s following a temperature step change. This is consistent with our observations, which suggest that the cold spike peaks at 0.2 s past the cloud exit point (Fig. 4). So Eq. (1) is the cloud exit EC bias fit for the section of 0.2–8.0 s past the cloud exit. For $0.0 < t < 0.2$ s, we use a linear function:

$$\Delta T = \Delta T_o \frac{t}{0.2} \qquad 0.0 < t < 0.2\,\text{s}. \quad (2)$$

The functions (1) and (2) describe the cloud exit EC well in most clean cases. We use this technique to obtain values of ΔT_o *and* τ_d for all cloud exits used in this study. An example of this fitting exercise is shown in Fig. 10. We define quality of fit as the mean of the absolute difference between the best-fit value and the measured value in the domain $0.0 < t < 8.0$ s. Table 1 shows the average quality of fit for all cloud exit regions. For each of the three experiments, the quality of fit averages at 0.10 K. This is an order of magnitude smaller than the average amplitude ΔT_o, also listed in Table 1. This amplitude is smallest in HiCu-03 (the coldest campaign) and highest in CuPIDO-06. On the other hand, the mean recovery time constant τ is largest

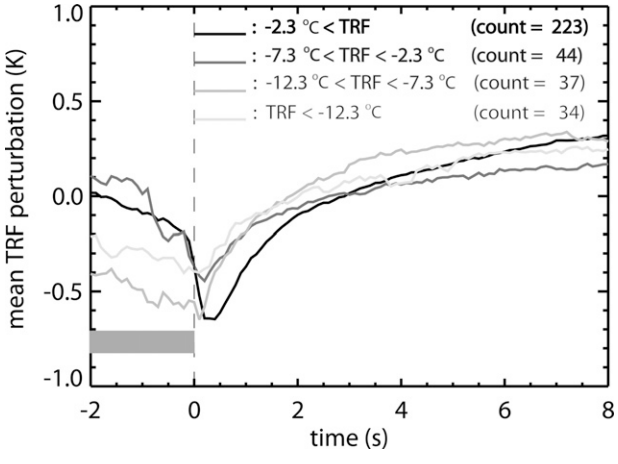

FIG. 9. Composite TRF traces for all clean cloud exits in the three campaigns, for four ambient temperature (T) ranges. The ambient temperature range is simply the 10-s mean TRF value. Note that −2.3°C corresponds to about 0.0°C in the RFT housing.

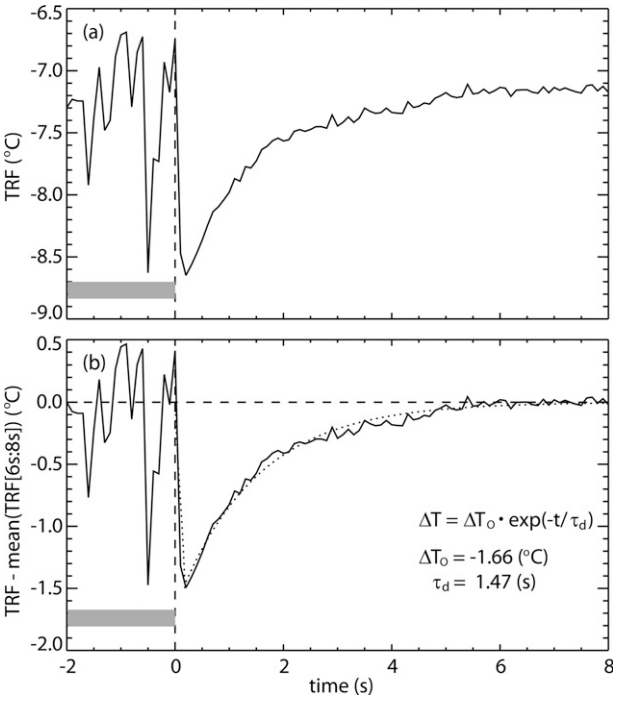

FIG. 10. (a) Illustration of the curve-fitting procedure for a cumulus exit in CuPIDO-06 (18 Jul 2006). (b) The negative of the cloud exit EC bias, and the dotted line is the best-fit curve to this bias. The curve fit parameters are listed.

in HiCu-03 and smallest in CuPIDO-06. In the next section, we show that these differences in both ΔT_o and τ_d can be interpreted mainly in terms of the relative dryness of the environment, expressed in terms of the wet-bulb depression.

c. *Factors affecting the cloud exit evaporative cooling bias*

We now examine what controls the two cloud exit EC bias parameters, ΔT_o and τ_d. We consider two environmental factors, the temperature and a measure of dryness outside the cloud. For the latter, we use the wet-bulb depression ($T_r - T_{w,\mathrm{ar}}$). (The symbols are explained in Fig. 7a.) We also consider four factors characterizing the cloud that was penetrated: N_o, LWC, the liquid water path (LWP, defined as the track-integrated LWC, in units g m^{-2}), and the mean droplet diameter ($\overline{D}$). The latter is derived from the 15 FSSP drop-size bins (5–50 μm). The cloud factors are averages or integrals over the entire cloud. The temperature is an average over the entire cloud exit vicinity, from 2 s inside cloud to 8 s outside cloud. The wet-bulb depression $T_r - T_{w,\mathrm{ar}}$ is an average between 0 and 2 s *before* the cloud entrance (i.e., on the other side of the cloud). The reason for this choice is not physical, but practical, as explained below.

The wet-bulb depression ($T_r - T_{w,\mathrm{ar}}$) applies to the dynamically heated air *inside* the RFT housing, as illustrated in Fig. 7a. It is computed from the pressure (p_r) and the temperature (T_r) inside the RFT housing, and the ambient mixing ratio w_a. Both T_r and w_a are measured. A LI-COR 6060 fast-rate w_a sensor was available in only two of the three campaigns (RICO-04 and CuPIDO-06), and displayed wetting symptoms itself in some cumulus penetrations. Therefore, we infer w_a from the slow-rate Cambridge chilled-mirror dewpoint sensor. The chilled-mirror w_a values in the entire exit region, well beyond the (exit point + 8 s), are contaminated by the cloud just penetrated, and they are in essence a surrogate for cumulus width. In a composite sense, the lowest chilled-mirror w_a values (those best representing the environment) occur just before the cloud entrance point, thus the wet-bulb depression is computed there. This solution is not ideal, because real humidity differences may occur on opposite sides of a cumulus, especially at a detrainment level.

The pressure p_r is derived as follows:

$$p_r = p_a + \Delta p = p_a + \frac{\rho r U_\infty^2}{2}. \tag{3}$$

Here U_∞ is the true airspeed of the aircraft, r is effective recovery factor of the RFT housing and sensing element (LC90) ($r = 0.625$ for the RFT on the WKA), p_a is the static air pressure at flight level (Fig. 7), and ρ is the air density. For the three field campaigns used in this study, the compression into the RFT housing (Δp) ranges between 20 and 24 hPa. The expression for wet-bulb depression (K) is (e.g., Pruppacher and Klett 1996, p. 490)

$$T_r - T_{w,\mathrm{ar}} = \frac{\mathrm{Le}(T_{w,\mathrm{ar}})\left[w_{\mathrm{SAT}}(T_{w,\mathrm{ar}}) - w_a\right]}{c_{\mathrm{pa}} + c_{\mathrm{pv}} w_a}. \tag{4}$$

Here $\mathrm{Le}(T_{w,\mathrm{ar}})$ is the latent heat of vaporization (J kg^{-1}) at temperature $T_{w,\mathrm{ar}}$, c_{pa} is the specific heat of air at constant pressure (J kg^{-1} K^{-1}), and c_{pv} is the specific heat of water vapor at constant pressure (J kg^{-1} K^{-1}). The term w_{SAT} in Eq. (4) is the saturation mixing ratio (kg kg^{-1}) at $T_{w,\mathrm{ar}}$:

$$w_{\mathrm{SAT}}(T_{w,\mathrm{ar}}) = \frac{\varepsilon e_{\mathrm{SAT}}(T_{w,\mathrm{ar}})}{p_r - e_{\mathrm{SAT}}(T_{w,\mathrm{ar}})}, \tag{5}$$

where $e_{\mathrm{SAT}}(T_{w,\mathrm{ar}})$ is the saturation vapor pressure (Pa) at $T_{w,\mathrm{ar}}$, and ε is a constant ($\varepsilon = 0.622$). There is no analytic solution for Eq. (4) for wet-bulb temperature, so it needs to be solved iteratively.

The exponential fit parameters ΔT_o and τ_d are plotted against the six factors for all clean cumulus exits in the three campaigns in Fig. 11. The three campaigns cover a broad spectrum of cumulus clouds, with a mean LWC ranging between 0.1 and 2.1 g m^{-3}, a mean N_o from 30 to 500 cm^{-3}, a mean $\overline{D}$ from 5 to 30 μm, and a mean flight-level temperature from −12.3°C (our threshold temperature) to +21°C.

The magnitude of the correlation coefficients[2] between LWP, N_o, and temperature on the one hand, and either ΔT_o or τ_d on the other, are all very low, less than 0.1 (Fig. 11). Surprisingly, neither the LWP (g m^{-2}) computed over the entire cloud (not shown) nor over the last 2 s before the exit point (shown) show a significant correlation. There is no clear lower-limit LWC or LWP for cloud exit EC to occur. This indicates that RFT sensor wetting happens rather readily, even for relatively thin or small liquid water clouds. With increasing cloud LWC, the amplitude of the cold spike ($|\Delta T_o|$) does tend to increase, suggesting that the wetting of the RFT sensor surface increases with LWC. In fact, the cumuli in CuPIDO-06 have both the largest LWC and the highest $|\Delta T_o|$, compared to those in the two other campaigns (Table 1). Still, the correlation

[2] The linear regressions and correlation coefficients are computed based on the minimization of the absolute differences (not the square of the differences) between observations and the regression line. This reduces the sensitivity to outliers.

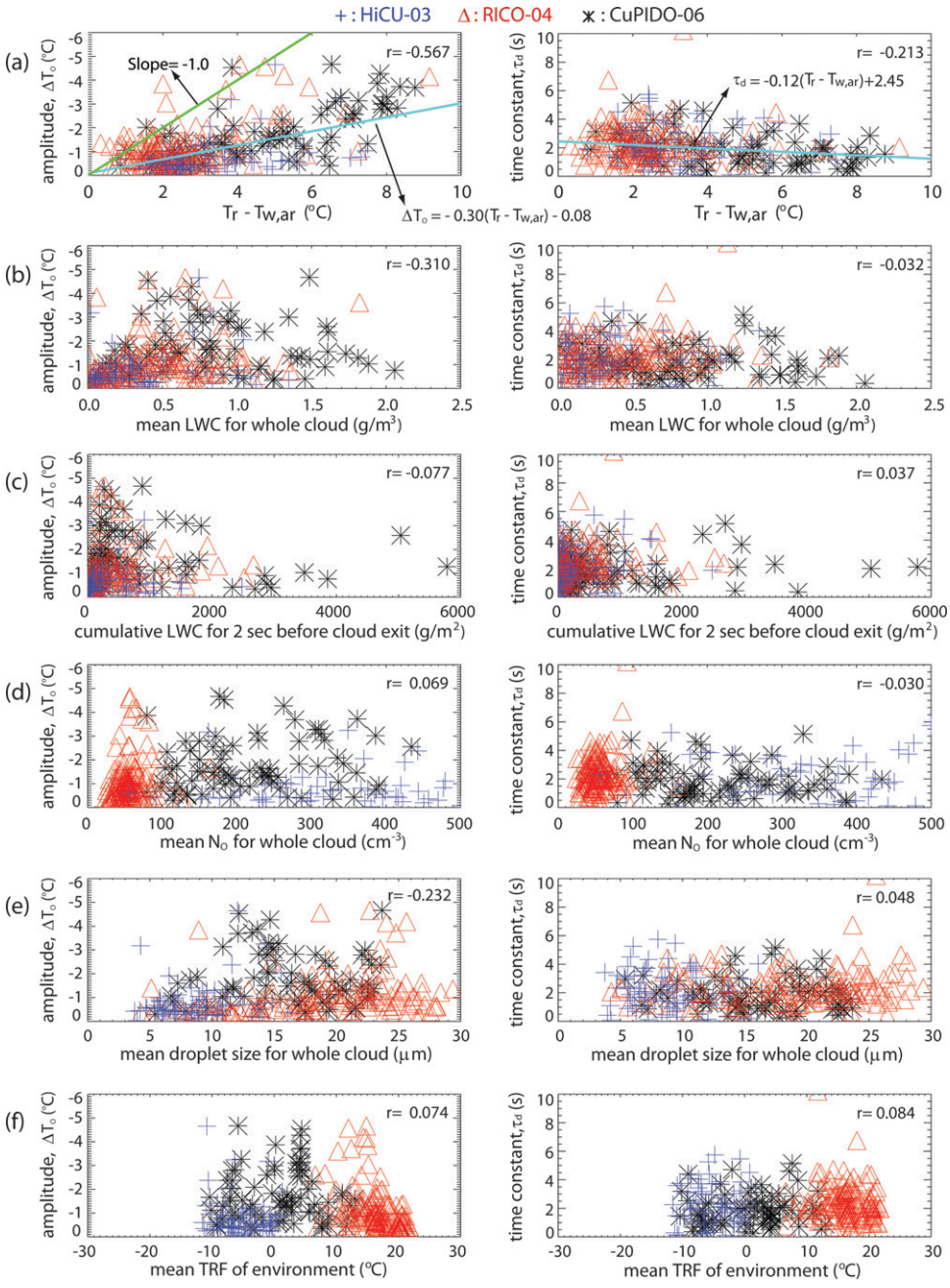

FIG. 11. Scatterplots of RFT cloud exit EC (left) bias amplitude (ΔT_o) and (right) time constant (τ_d) vs six cloud and environmental parameters, for all clean cloud exits in three experiments with ambient temperatures of at least −12.3°C. (a) The linear regression equation and line are shown for both parts. The correlation coefficient r is shown in each scatterplot.

with LWC shown in Fig. 11b is poor and dominated by outliers. There seems to be a threshold value of N_o for EC to occur, but this simply arises from the definition of a cloud, based on the threshold value $N_{o,c}$, as discussed in section 2. (Some points in Fig. 11d have a mean $N_o < N_{o,c}$ because these clouds have one or more small cloud breaks, less than 100 m wide.) There is a weak tendency for EC to be larger, and thus the wetting of the RFT sensor surface to be more complete, when the mean drop size $\overline{D}$ is larger (Fig. 11e). A clear negative correlation between $\overline{D}$ and $|\Delta T_o|$ would indicate that the sensor wetting is the result of small droplets that remain suspended in the flow that reverses and enters the RFT cylinder. The absence of such a nega-

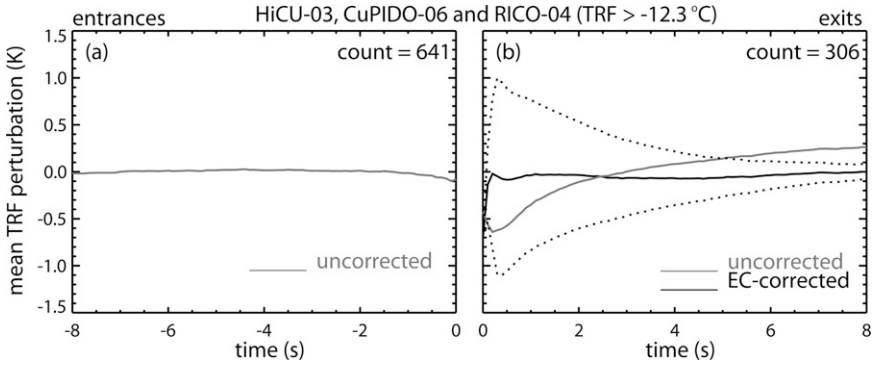

FIG. 12. Composite TRF traces for all clean (a) cloud entrances and (b) cloud exits in three campaigns. The values shown are perturbations from the 8-s mean for each entrance or exit region. Gray lines denote the uncorrected, original TRF, black lines the TRF with a correction for EC in the exit region. The black dotted lines are the mean corrected values ±1 standard error.

tive correlation suggests that water shedding from the RFT housing (an idea proposed by LC90) is important.

In short, no single cloud or environmental factor explains cloud exit EC. The wet-bulb depression $T_r - T_{w,\mathrm{ar}}$ is most strongly correlated: the drier the environment, the larger the cooling spike ΔT_o and the smaller τ_d (i.e., the more rapidly the droplets evaporate from the platinum wire). The linear regression between ΔT_o and the wet-bulb depression is as follows:

$$\Delta T_{\mathrm{o}} = -0.30\left(T_r - T_{w,\mathrm{ar}}\right) - 0.08 \qquad (\mathrm{K}). \quad (6)$$

This means that upon exiting a cloud, TRF is cooled to 30% of its potential by evaporation [i.e., the ambient wet-bulb depression (Fig. 8)]. The full wet-bulb depression can only be attained if the platinum wire spiral is and remains fully wet. Only for a few cumulus penetrations was this potential reached, according to Fig. 11a. The standard error[3] for linear regression (6) is 0.80 K. This is a measure of uncertainty of the EC correction in the cloud exit region. Similarly, the linear regression between τ_d and the wet-bulb depression is as follows:

$$\tau_d = -0.12\left(T_r - T_{w,\mathrm{ar}}\right) + 2.45 \qquad (\mathrm{s}). \quad (7)$$

Regression Eqs. (6) and (7) were evaluated for various samples of the entire population of clean cloud exits, in order to find contrasts and stronger correlations. These samples included the three different campaigns, maritime versus continental clouds, and cold versus warm clouds. None of the regression equations are substantially different, none of the correlation coefficients are substantially higher, and none of the remaining uncertainty is substantially lower. Compare, for instance, the standard errors of ΔT_o for each of the campaigns (Table 1) with those for the three campaigns combined. We also tried multiple regressions with the top two and three variables, in terms of their correlation with ΔT_o (Fig. 11). These regressions are not significantly better either. Therefore we propose that Eqs. (1) and (2) are used to correct the TRF values for EC in the cloud exit region, with the amplitude ΔT_o given by Eq. (6) and the drying time τ_d given by Eq. (7). The latter two equations represent the entire sample size and the broadest parameter space. The full correction is applied at mean temperatures above −2.3°C, no correction is applied below −12.3°C, and a fraction of the correction increasing linearly between 0% and 100% is applied between −12.3° and −2.3°C.

To test this correction, a TRF composite for all entrances and all exits with TRF > −12.3°C is shown in Fig. 12. Here we focus on the correction outside of cloud. The values plotted in Fig. 12 are departures from the 10-s mean; thus what matters is the slope of the curve, starting far away from the cloud. The composite corrected temperature traces in the clear air are rather flat in the cloud entrance and cloud exit cases, confirming the validity of the cloud exit EC bias correction. The temperature decreases slightly toward cloud (~0.1 K) in the cloud entrance region. Such cooling may be present in the exit region also, near $t = 0.5$ s in Fig. 12b, but it is masked by the much larger EC correction. This cloud edge cooling may well be real. It may be due to the evaporative cooling of detrained cloudy parcels, or to radial variation of adiabatic warming (e.g., subsidence that peaks some distance away from the cloud edge). In any event, the similarity of the exit and entrance TRF trends gives confidence in the EC correc-

[3] The standard error is the standard deviation of the difference between the linear regression values and the true values.

tion. The standard error, shown in Fig. 12b, reflects the uncertainty in the EC correction only, not the overall RFT instrument uncertainty. It is computed from the standard errors of both the ΔT_o and τ_d estimates (i.e., it is based on the scatter around the regression curves in both parts of Fig. 11a).

4. Reverse flow temperature correction in cloud

Clearly, the true temperature in cumuli varies substantially, more than in the surrounding clear air, as is evident in the larger standard deviations in cloud than out of cloud in Fig. 4. But the dependence of the in-cloud temperature trend within 200 m of the cloud edge on the flight direction (into or out of the cloud) in a large composite of cases (Fig. 4) is an indication of an instrument bias. We now demonstrate that the EC correction proposed for cloud exit regions (section 3c) can also be used to estimate the TRF bias within cumulus clouds and to remove the erroneous cooling trend from entrance point to exit point.

Within a cumulus cloud, the dynamically heated air in the RFT housing is subsaturated, leading to EC of a wetted surface. We make the following three assumptions:

1) The cloudy air is saturated, that is, the relative humidity is precisely 100%. This implies that the vapor pressure in cloud equals the saturation vapor pressure at the best temperature estimate available (i.e., the EC-corrected TRF, denoted as TRFc).
2) The water vapor mixing ratio in the RFT housing equals that in the cloudy-free airstream (i.e., droplets do not have a chance to evaporate in the dynamically heated air). This implies that the wet-bulb depression equals the difference between dynamically heated temperature (T_r) and the wet-bulb temperature $T_{w,\mathrm{cr}}$ (Fig. 7a), or successive corrections of that difference (Fig. 7b).
3) Evaporative cooling of the RFT sensor in cloud occurs at the same fraction of the wet-bulb depression as observed just outside a cloud [i.e., Eq. (6) applies in-cloud as well]. This assumption is rather conservative, because the cloud exit cold spike magnitude is constrained by sensor drying outside cloud, and reaches only 30% of the wet-bulb depression, whereas continuous sensor wetting occurs within cloud.

More specifically, the third assumption applies everywhere in cloud except near the entrance. Individual transects, and composites such as the one for the RICO-04 entrance cases (Fig. 4g), suggest that the wetting of the RFT sensor just beyond the cloud entrance and the resulting cooling is a rapid process, but is not instantaneous. The composite TRF signature at the entrance region shows some initial warming, followed by cooling farther in the cumulus. We interpret the initial warming as real and the follow-up cooling as dominated by EC. Theoretically the composite TRF trace for all the entrances should be very similar to that for all the exits. Thus we choose the RTF ''wetting time constant'' τ_w as 0.7 s. This value is chosen by trial and error, comparing the corrected composite TRF trace following cloud entrance with that before cloud exit (shown below). We use an exponential adjustment like Eq. (1), with τ_w as the time constant and the full in-cloud correction derived below as the amplitude. The use of an exponential rather than a linear curve is somewhat arbitrary, and is motivated by the idea that the probability of a new drop being collected by the platinum spiral wire decreases with the number of droplets already present on the wire.

The in-cloud correction is an iterative process, as follows: the initial guess for TRFc equals T_c, which is corrected for dynamic heating (Fig. 7b) but not for EC. The wet-bulb temperature $T_{w,cr}$ then is calculated as

$$T_{w,\mathrm{cr}} = T_r + (\mathrm{TRFc} - T_c) - \frac{\mathrm{Le}(T_{w,\mathrm{cr}})\left[w_{\mathrm{SAT}}(T_{w,\mathrm{cr}}) - w_c\right]}{c_{\mathrm{pa}} + c_{\mathrm{pv}} w_c}, \quad (8)$$

where w_c is water vapor mixing ratio (kg kg^{-1}) in cloud, computed as the saturation mixing ratio at the dewpoint temperature in cloud (TRFc),

$$w_c = \frac{\varepsilon e_{\mathrm{SAT}}(\mathrm{TRFc})}{p_a - e_{\mathrm{SAT}}(\mathrm{TRFc})}.$$

In Eq. (8), w_{SAT} is the saturation mixing ratio at $T_{w,\mathrm{cr}}$:

$$w_{\mathrm{SAT}}(T_{w,\mathrm{cr}}) = \frac{\varepsilon e_{\mathrm{SAT}}(T_{w,\mathrm{cr}})}{p_r - e_{\mathrm{SAT}}(T_{w,\mathrm{cr}})}.$$

The term $T_r + (\mathrm{TRFc} - T_c)$ in Eq. (8) is explained as follows: the EC correction changes the estimate of the free-airstream temperature from T_c to TRFc. This correction also applies inside the RFT housing; in other words the estimate of the dynamically heated air changes from T_r to $T_r + (\mathrm{TRFc} - T_c)$ (Fig. 7b). Following assumption (3) above, we obtain a new TRFc based on Eq. (6):

$$\mathrm{TRFc} = T_c + 0.30\left[T_r + (\mathrm{TRFc} - T_c) - T_{w,\mathrm{cr}}\right] \times \left[1 - \exp\left(\frac{-t}{\tau_w}\right)\right] + 0.08, \quad (9)$$

where t is time, computed from the cumulus entrance point and increasing into the cloud. We then compare

TRFc from Eq. (9) with its initial guess (T_c), and iterate through Eqs. (8) and (9) until the successive values of TRFc differ by less than 0.001 K. At that point, TRFc = T_{cf}, and the temperature in the RFT housing is T_{rf}, following the notation in Fig. 7b. Note that the correction proposed herein is different for aircraft flying at different operational speeds. Section 3 in LC90 can be used as a guide to adapting our correction to different airspeeds.

An example of the EC correction of TRF is shown in Fig. 13 for an isolated cumulus. The gradual development of this correction as the aircraft penetrates into cloud can be seen. The in-cloud correction ranges between +0.1 and +0.6 K, averaging 0.40 K. This correction is smaller than the correction in the cloud exit region, because the wet-bulb depression (in the RFT housing) inside the cloud is smaller than that in the clear air, but it is not insignificant.

The overall impact of the EC correction of TRF on temperature estimation in cumulus clouds is summarized in the three-campaign composite (Fig. 14). The composite temperature trends from the cloud edge to the interior are similar for entrance and exit regions. Instead of a cooling trend from entrance to exit points, there is some cooling from the cloud core to both cloud edges. On average the EC correction in cloud amounts to a warming of 0.46 K in all clean clouds used in this study, except close to the cloud entrances, where the correction is smaller. The standard error in cloud (shown in Figs. 14a,b) is computed in the same way as that for the cloud exit region, that is, it is based on the uncertainty of both ΔT_o and τ_d, but only within the range of wet-bulb depressions encountered in the RFT housing in cloud.

The uncorrected TRF in cloud tends to be lower than that in the environment, both in the exit and entrance regions (Fig. 14d). The EC-corrected composite temperature is higher. Also, the highest temperatures are found toward the cumulus core, as one would intuitively expect. This implies that if one isolates the temperature perturbation term in the expression for buoyancy, clouds now are positively buoyant, whereas the original TRF trace suggests that they are negatively buoyant. This is explored further in the next section.

5. Discussion

The proposed correction of TRF for EC in and just outside clouds is important in the study of cumulus dynamics. We now illustrate that, without the correction, cumulus buoyancy is underestimated and entrainment rate overestimated.

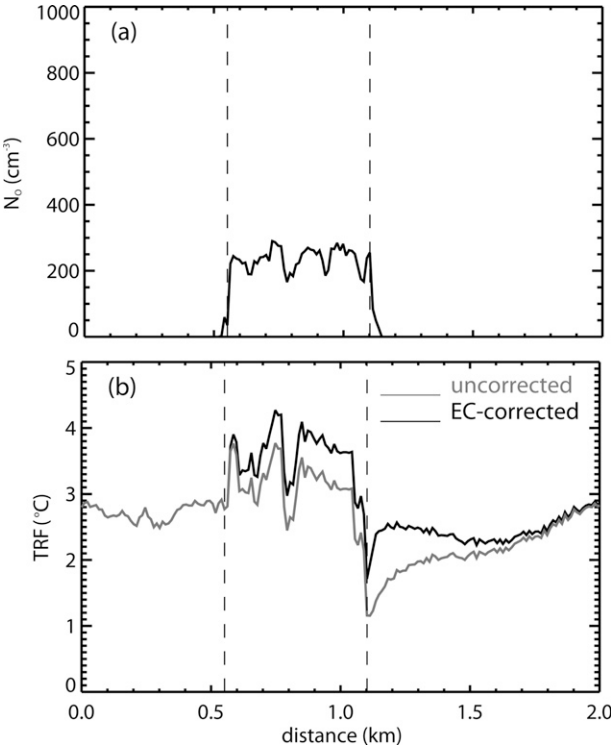

FIG. 13. Illustration of the in-cloud and cloud exit EC bias corrections for an isolated cumulus in CuPIDO-06 at 1637:02 UTC 17 Aug 2006: (top) N_o and (bottom) TRF.

a. Buoyancy

The buoyancy B (m s^{-2}) is computed as follows (e.g., Houze 1993):

$$B = g\left(\frac{\theta'}{\theta_o} + 0.61w_v' - \frac{c_v}{c_p}\frac{p'}{p_o} - w_H\right), \qquad (10)$$

where θ is the potential temperature (K) and w_H is the mixing ratio of liquid and/or frozen water (kg kg^{-1}). The parameters with a prime ($'$) represent the deviation from the reference values, while the ones with subscript o denote the reference states. The environment surrounding a cumulus cloud represents the reference state. We compute the reference temperature as the average value in the clear air surrounding the cloud. For the two cases shown in Fig. 15, the available clear air region at the same flight level is −500 to 0 m on the uptrack side of the cumulus, and +500 to +2000 m on the downtrack side. Because of the slow response of the chilled mirror dewpoint sensor (see section 3c), the reference water vapor mixing ratio w_v is computed over 500 m in the entrance region only. Within cloud, the air is assumed to be precisely saturated, thus $w_v = w_{v,\mathrm{SAT}}$ (T_{cf}). An upward correction of temperature affects buoyancy in two ways: it increases the first term on the

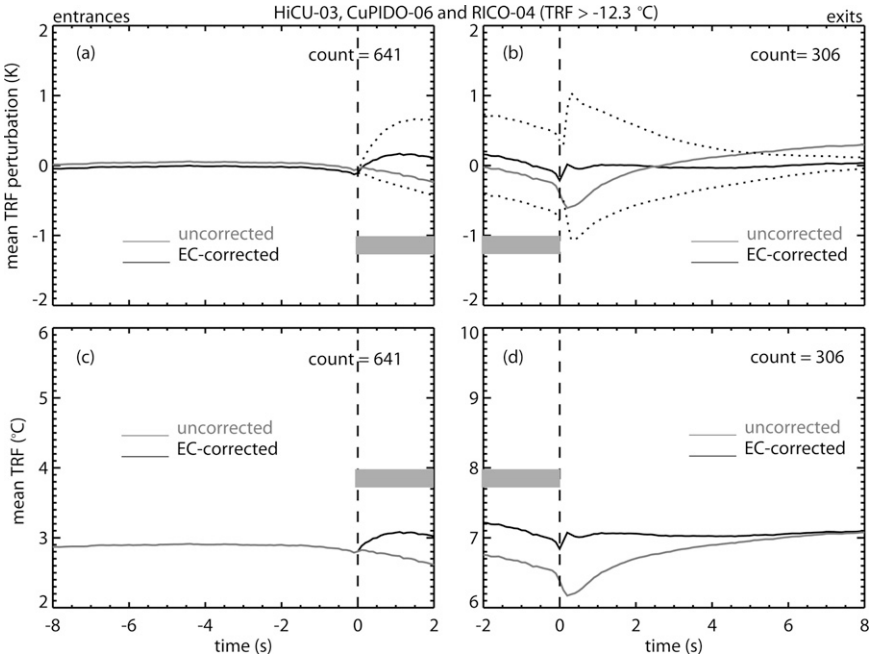

FIG. 14. (a), (b) As in Fig. 12, but with the EC correction applied both in cloud and cloud exit regions. Again, the dotted lines are the mean corrected values ±1 standard error. (c), (d) As in (a), (b), but the actual average temperature is shown, rather than the average departure from each individual 10-s mean.

right and also the second term, because a higher temperature implies a higher saturation mixing ratio. The hydrometeor loading term w_H is computed from the water mass in the FSSP and the 2D optical array probes. The pressure perturbation term [third on the right in Eq. (10)] is ignored because the altitude of the aircraft is not known with enough precision.

According to (10), 0.5 K of excess heat (θ') produces the same buoyancy as ~3 g kg^{-1} of excess water vapor and ~1.6 g kg^{-1} of water loading w_H. (The latter is negative buoyancy.) Thus, an in-cloud TRF correction of +0.5 K is significant. To illustrate the impact of the correction on buoyancy calculations, we examine two penetrations of vigorous, growing cumuli in CuPIDO-06 (Fig. 15). This illustration includes the reflectivity and Doppler velocity transects from the Wyoming Cloud Radar (WCR). The WCR operated in a vertical plane above and below the aircraft (Damiani et al. 2008). The narrow horizontal black stripe in Figs. 15a,b,e,f indicates the radar blind zone (~100-m range, both up and down). The flight level is centered in this blind zone. The radar data provide a vertical slice of the cumulus and assist in the interpretation of the flight-level data. In both cases updrafts exceeded 10 m s^{-1} at and below flight level. The penetrations occurred about 1 km below cloud top but above the freezing level. An older cumulus with strong downward motions (near $x =$ 0.5 km in Fig. 15b) is collapsing just to the left of the first target cumulus. The high reflectivity below flight level (Fig. 15a) is attributed to precipitation-size particles. Our interest is in the updraft plume at $1.0 < x < 2.0$ km, extending from near the cloud base to the top (Fig. 15b). It is flanked by subsidence on both sides, near $x = 2.5$ and $x = 0.5$ km (Figs. 15b,d). The EC bias correction increases the in-cloud temperature, resulting in a significant increase in cloud buoyancy. The uncorrected buoyancy values are negative on average, which is difficult to reconcile with the updraft strength measured at flight level and over the depth of the cloud. The corrected buoyancy is mostly positive across the updraft plume (except for the right flank of the updraft, near $x \leq 2.0$ km). The cumulus on the right (Fig. 15e) probably is younger since its reflectivity is lower, but it has an even stronger updraft plume bubbling up to flight level (near $1.5 < x < 2.0$ km in Figs. 15f,h). The uncorrected buoyancy is slightly negative over the width of this cloud. As a result of the EC correction, this updraft plume again becomes mostly positively buoyant, in particular in the updraft region (Fig. 15g).

The impact of the EC correction on the composite buoyancy for all clean cloud edges is shown in Fig. 16. Here the reference temperature and mixing ratio are computed as the average over the 10 s shown (2 s in cloud and 8 s out of cloud). The pressure perturbation

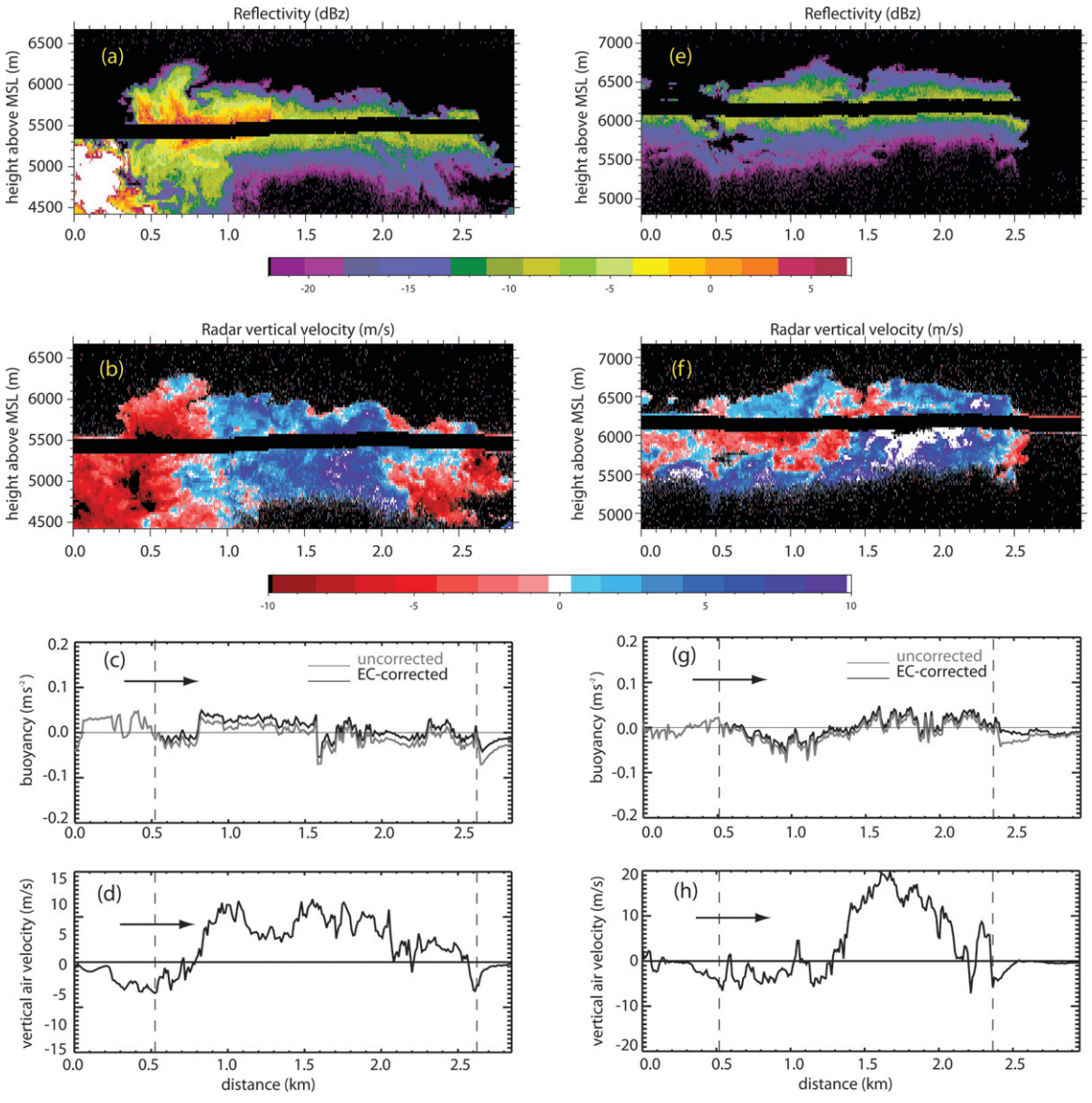

FIG. 15. An illustration of the impact of the TRF correction on buoyancy for two CuPIDO-06 cumuli, at (left) 1806:56 and (right) 1936:52 UTC 2 Aug 2006. (top colored panels) WCR profiles centered at flight level (black stripe): (top) reflectivity and (bottom) vertical velocity. The aspect ratio of these cross sections is 3.6:1. (bottom graphs) Flight-level data with the vertical dashed lines indicate the cumulus (left) entrance and (right) exit points, as determined from FSSP data: (top) buoyancy and (bottom) vertical air velocity.

term in (10) is ignored again, and the mixing ratio is assumed to be saturated in cloud. This assumption affects the water vapor term in (10) and explains the jump in buoyancy at both cloud edges in Fig. 16. The uncorrected TRF yields negatively buoyant cloud cores on average, inward from the entrance point (Fig. 16a). This applies even for the subset of cases where the average vertical velocity in cloud is positive (not shown). The uncorrected composite buoyancy decreases from cloud entrance to exit, driven by the same trend in the uncorrected TRF trace (Fig. 14). The buoyancy discontinuity at the inner cloud (where Figs. 16a,b meet) is simply due to the definition of buoyancy, whose reference is just the average of the 10-s trace, for convenience. In any event, the use of the EC-corrected TRF yields higher buoyancy in the cloud's core.

b. Entrainment

The impact of the EC correction on entrainment estimates is illustrated by means of a Paluch diagram (Paluch 1979) (Fig. 17). The CuPIDO experiment benefitted from excellent proximity soundings collected by

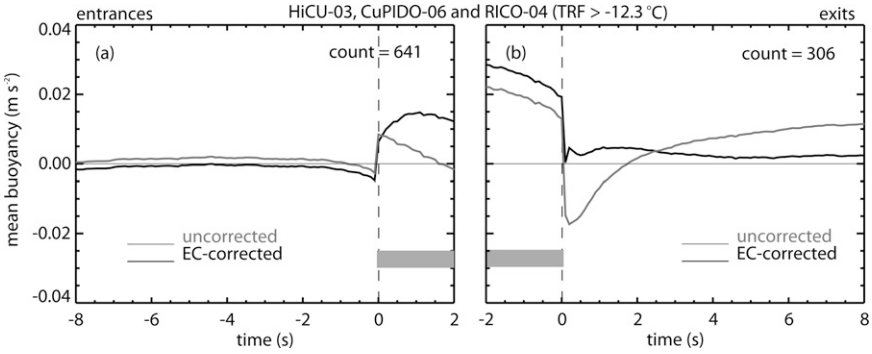

FIG. 16. Composite buoyancy in (a) cloud entrance and (b) cloud exit regions.

a Mobile GPS Advanced Upper-Air Sounding (M-GAUS) system. The radiosondes were released about 10 km upstream of the target orographic cumulus in both examples in Fig. 17, and they ascended in clear air within minutes of the aircraft cloud penetration. We verified that the radiosonde did not penetrate the cloud at any level. Two variables conserved under pseudo-adiabatic moist processes are plotted: θ_q, the wet equivalent potential temperature (defined in Paluch 1979), and w_{TOT}, the total water mixing ratio. As before, the mixing ratio in cloud (i.e., the aircraft data) is assumed to be its saturated value. Also shown in Fig. 17 are the cloud base (corresponding with the soundings' lifting condensation level) and the cloud top (inferred from WCR up-antenna reflectivity and photostereogrammetry; see Zehnder et al. 2007). Undiluted cloud parcels ascending from below have the properties of the air at cloud base; mixtures of undiluted boundary layer air with air from above the cloud (i.e., vertical entrainment) fall on the line connecting cloud base to cloud top in Fig. 17. The closer the in-cloud measurements are to the sounding curve at flight level, the stronger the lateral entrainment at that level. The effect of the EC correction is to increase θ_q by 1.6 K in the warm cloud (Fig. 17a). In the colder cloud (Fig. 17b), the θ_q increase is smaller, because of the temperature dependence of the EC correction (section 3c). The total water w_{TOT} increases as well, since air in cloud is assumed to be saturated. Thus the in-cloud measurements in Fig. 17 move slightly downward, and mainly to the right. In the case of the deeper cloud (Fig. 17b) more vertical entrainment is apparent, and in the more shallow cumulus (Fig. 17a) the sampled air is more similar to the cloud-base air. In summary, the use of uncorrected TRF values tends to exaggerate lateral entrainment.

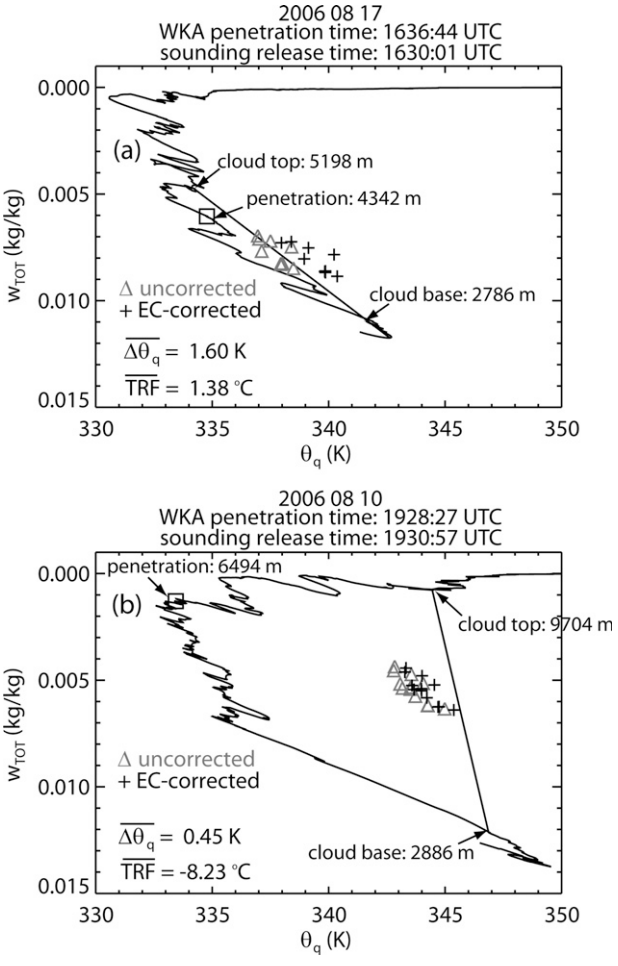

FIG. 17. Paluch diagram for two cases during CuPIDO-06. The lines represent M-GAUS sounding data; the triangle and + symbols are aircraft data. The square symbol represents the sounding data corresponding to the flight altitude. The mean change in wet equivalent potential temperature ($\overline{\Delta\theta_q}$) resulting from the EC correction and the mean temperature ($\overline{\mathrm{TRF}}$) are listed.

c. *Further implications*

Several studies have estimated cumulus buoyancy and/or entrainment using a reverse-flow thermometer

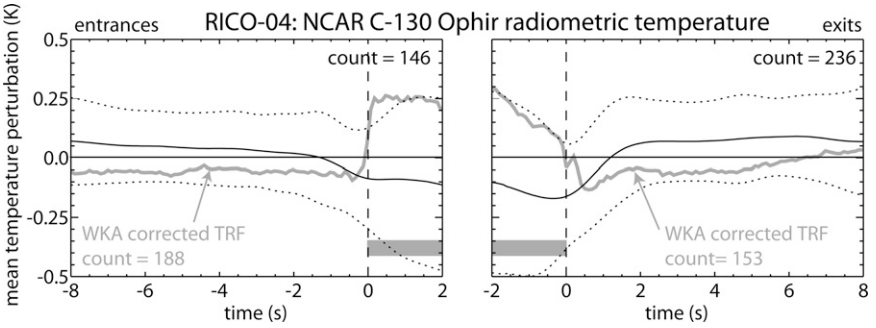

FIG. 18. Composite Ophir temperature for all clean cloud penetrations by the NCAR C-130 aircraft during RICO-04. The average and the average ±1 std dev are shown. The bold gray line is the composite corrected TRF trace for all RICO-04 cloud penetrations by the WKA, shown for comparison.

on an aircraft flying at about the same speed as the WKA (~100 m s^{-1}); these include Boatman and Auer (1983), Austin et al. (1985), Jensen et al. (1985), Blyth et al. (1988), and Damiani et al. (2006). In some papers other variables were derived from TRF, for instance, equivalent potential temperature (Heymsfield et al. 1978). The EC correction proposed herein should be applied to all those studies. Since most of the measurements in the papers listed above occurred at temperatures above −12°C, their analyses are affected and some of their conclusions may be flawed. A further investigation is worthwhile.

It should further be noted that while airborne *radiometric* thermometers avoid the issue of evaporative cooling, they have their own problems near cloud and precipitation (e.g., Nicholls et al. 1988; Jorgensen and LeMone 1989). To illustrate this, we plotted the composite temperature trace from the Ophir radiometric thermometer on the NCAR C-130 aircraft in RICO-04 (Fig. 18). Clearly the C-130 did not penetrate the same cumuli at the same time as the WKA, but it flew at overlapping times, in the same region as the WKA, and it also penetrated the cumuli from random directions, often along great circles drifting with the wind. The composite Ophir in-cloud temperature was about 0.2 K *lower* than the ambient air temperature, while the corrected RFT in-cloud temperature was about 0.3 K *higher* than the surrounding clear air. The implications for cumulus buoyancy are obvious. For the Ophir it is likely that the in-cloud temperature measurement is more accurate, because of the lower transmittance of radiation in the Ophir CO_2 infrared absorption band in cloudy air.

6. Conclusions

There is strong evidence that the sensor of an airborne reverse-flow immersion thermometer (RFT) becomes partially wetted in cloud, notwithstanding the reverse flow design. Aircraft data collected during numerous penetrations of cumulus clouds in a broad range of environmental and cloud conditions have been used to estimate the bias of an RFT due to evaporative cooling both in the cloud exit region and within cloud. The following results have been reached:

1) A cold spike is commonly encountered as the aircraft exits the cloud. Because such a spike is not present in the cloud entrance region, it must be due to evaporative cooling on a wetted sensor.
2) The amplitude of this cold bias varies much and does not strongly correlate with cloud or environmental conditions, but it is about 30% of the wet-bulb depression of the ambient air.
3) This cloud exit temperature bias can be used to correct RFT values within clouds. This correction increases the cloud temperatures by 0.4–0.5 K. Previous work using RFT measurements underestimated the buoyancy and overestimated the entrainment in cumulus clouds.

In further work we will use the proposed RFT correction for evaporative cooling to study buoyancy and entrainment in the context of fundamental cumulus dynamics.

Acknowledgments. This work was supported by National Science Foundation Grant ATM-0444254. We appreciate the anonymous reviews and the insightful discussions with Alfred R. Rodi, Jeffrey French, Gabor Vali, Larry Oolman, and Perry Wechsler.

REFERENCES

Austin, P., M. Baker, A. Blyth, and J. Jensen, 1985: Small-scale variability in warm continental cumulus clouds. *J. Atmos. Sci.,* **42,** 1123–1138.

Blyth, A. M., 1993: Entrainment in cumulus clouds. *J. Appl. Meteor.,* **32,** 626–641.

——, W. A. Cooper, and J. B. Jensen, 1988: A study of the source of entrained air in Montana cumuli. *J. Atmos. Sci.,* **45,** 3944–3964.

Boatman, J. F., and A. H. Auer, 1983: The role of cloud top entrainment in cumulus clouds. *J. Atmos. Sci.,* **40,** 1517–1534.

Brenguier, J., D. Baumgardner, and B. Baker, 1994: A review and discussion of processing algorithms for FSSP concentration measurements. *J. Atmos. Oceanic Technol.,* **11,** 1409–1414.

Damiani, R., G. Vali, and S. Haimov, 2006: The structure of thermals in cumulus from airborne dual-Doppler radar observations. *J. Atmos. Sci.,* **63,** 1432–1450.

——, and Coauthors, 2008: The Cumulus, Photogrammetric, In Situ, and Doppler Observations experiment of 2006. *Bull. Amer. Meteor. Soc.,* **89,** 57–73.

Eastin, M. D., P. G. Black, and W. M. Gray, 2002: Flight-level thermodynamic instrument wetting errors in hurricanes. Part I: Observations. *Mon. Wea. Rev.,* **130,** 825–841.

Geerts, B., Q. Miao, and J. C. Demko, 2008: Pressure perturbations and upslope flow over a heated, isolated mountain. *Mon. Wea. Rev.,* **36,** 4272–4288.

Gerber, H., B. G. Arends, and A. S. Ackerman, 1994: New microphysics sensor for aircraft use. *Atmos. Res.,* **31,** 235–252.

Heymsfield, A. J., P. N. Johnson, and J. E. Dye, 1978: Observations of moist adiabatic ascent in northeast Colorado cumulus congestus clouds. *J. Atmos. Sci.,* **35,** 1689–1703.

——, J. E. Dye, and C. J. Biter, 1979: Overestimates of entrainment from wetting of aircraft temperature sensors in cloud. *J. Appl. Meteor.,* **18,** 92–95.

Houze, R. A, Jr, 1993: *Cloud Dynamics*. Academic Press, 573 pp.

Jensen, J., P. Austin, M. Baker, and A. Blyth, 1985: Turbulent mixing, spectral evolution and dynamics in a warm cumulus cloud. *J. Atmos. Sci.,* **42,** 173–192.

Jonas, P. R., 1990: Observations of cumulus cloud entrainment. *Atmos. Res.,* **25,** 105–127.

Jorgensen, D. P., and M. A. LeMone, 1989: Vertical velocity characteristics of oceanic convection. *J. Atmos. Sci.,* **46,** 621–640.

King, W. D., C. T. Maher, and G. A. Hepburn, 1981: Further performance tests on the CSIRO liquid water probe. *J. Appl. Meteor.,* **20,** 195–202.

LaMontagne, R. G., and J. W. Telford, 1983: Cloud top mixing in small cumuli. *J. Atmos. Sci.,* **40,** 2148–2156.

Lawson, R. P., and A. R. Rodi, 1987: Airborne tests of sensor wetting in a reverse flow temperature probe. *Proc. Sixth Symp. on Meteorological Observation and Instrumentation,* New Orleans, LA, Amer. Meteor. Soc., 253–256.

——, and W. A. Cooper, 1990: Performance of some airborne thermometers in clouds. *J. Atmos. Oceanic Technol.,* **7,** 480–494.

LeMone, M. A., 1980: On the difficulty of measuring temperature and humidity in cloud: Comments on ''Shallow convection on day 261 of GATE: Mesoscale arcs.'' *Mon. Wea. Rev.,* **108,** 1702–1705.

Lenschow, D., and W. Pennell, 1974: On the measurement of in-cloud and wet-bulb temperatures from an aircraft. *Mon. Wea. Rev.,* **102,** 447–454.

McCarthy, J., 1974: Field verification of the relationship between entrainment rate and cumulus cloud diameter. *J. Atmos. Sci.,* **31,** 1028–1039.

Nicholls, S., E. L. Simmons, N. C. Atkins, and S. D. Rudman, 1988: A comparison of radiometric and immersion temperature measurements in water clouds. *Proc. 10th Int. Conf. on Cloud Physics*, Hamburg, Germany, International Commission on Clouds and Precipitation, 322–324.

Paluch, I. R., 1979: The entrainment mechanism in Colorado cumuli. *J. Atmos. Sci.,* **36,** 2467–2478.

Politovich, M. K., and W. A. Cooper, 1988: Variability of the supersaturation in cumulus clouds. *J. Atmos. Sci.,* **45,** 1651–1664.

Pruppacher, H. R., and J. D. Klett, 1996: *Microphysics of Clouds and Precipitation*. Kluwer, 954 pp.

Rauber, R. M., and Coauthors, 2007: Rain in (shallow) Cumulus over the Ocean—The RICO campaign. *Bull. Amer. Meteor. Soc.,* **88,** 1912–1928.

Rodi, A. R., and P. A. Spyers-Duran, 1972: Analysis of time response of airborne temperature sensors. *J. Appl. Meteor.,* **11,** 554–556.

Spyers-Duran, P. A., and D. Baumgardner, 1983: In flight estimation of the time response of airborne temperature sensors. *Proc. Fifth Symp. on Meteorological Observation and Instrumentation,* Toronto, ON, Canada, Amer. Meteor. Soc., 352–357.

Zehnder, J. A., J. Hu, and A. Razdan, 2007: A stereo photogrammetric technique applied to orographic convection. *Mon. Wea. Rev.,* **135,** 2265–2277.